DOI: 10.19884/j.1672-5220.202403002

Effect of Thermo-Oxidative Aging on Flexural Behavior of Quasi-Isotropic Carbon Fiber Reinforced Composite Laminates

SHAKYA Priyanka, GU Bohong*
Shanghai Frontier Science Research Center for Modern Textiles, College of Textiles, Donghua University, Shanghai 201620, China

Abstract: With an increased utilization of carbon fiber reinforced polymers (CFRPs) in high temperature environments, investigating their effects on materials becomes exceedingly important. This study presents a comparative investigation of thermo-oxidative aging effects on the flexural performance of two carbon fiber reinforced composite laminates (CFRCLs): a quasi-isotropic plain-woven CFRCL and a quasi-isotropic unidirectional layup CFRCL (designated as PW-CFRCL and UD-CFRCL, respectively). The CFRCLs were subjected to thermo-oxidative aging for specific durations, and their flexural strength was evaluated through three-point bending tests. The flexural strength of the laminates decreased with the prolonged aging duration. Despite having lower fiber content, PW-CFRCLs showed higher flexural strength than UD-CFRCLs. After eight days of aging, the flexural strength of PW-CFRCLs decreased by merely 4%–5%, while that of UD-CFRCLs decreased by 11%–14%. After 32 days of aging, the thinner PW-CFRCL with the lowest fiber content exhibited the highest flexural strength (595.52 MPa), followed by the thinner UD-CFRCL (549.83 MPa), then the thicker PW-CFRCL (445.29 MPa) and finally, the thicker UD-CFRCL (393.90 MPa). The decline in flexural properties of the laminates was primarily attributed to matrix cracking and interface debonding resulting from matrix oxidation. To validate the universality of this result, the finite element method was employed, showing a good correlation with the experimental findings.

Keywords: flexural strength; thermo-oxidative aging; matrix oxidation; interface debonding; finite element method
CLC number: TB332 **Document code**: A
Article ID: 1672-5220(2025)03-0259-14

Open Science Identity (OSID)

0 Introduction

The application of carbon fiber reinforced polymers (CFRPs) has been gaining prevalence in industries such as aerospace, automotive, marine, wind energy and pressure vessels[1-4]. These sectors often expose composites in challenging environments with intricate loading conditions[5-6], such as thermal, oxidative and mechanical coupling loadings[7]. Polymer matrix composites, including CFRPs, demonstrate susceptibility to heat and oxygen, resulting in intensive thermal oxidation after prolonged exposure[8], leading to the formation of oxidation byproducts close to the exposed surfaces, thereby contributing to volume shrinkage of the matrix[9] and damage cracks[10]. Although fibers retain structural integrity, interface degradation arises due to the development of volumetric shrinkage, strain and stress fields in the fiber/matrix interface, culminating in material failure characterized by delamination[11-12]. Compared with traditional metallic materials, the lower thermal conductivity of CFRPs exacerbates their susceptibility to heat. This thermal limitation becomes an essential consideration when utilizing CFRPs in applications where significant temperature variations prevail.

Oxidation fundamentally occurs on the composite surface. Discrepancies in the coefficients of thermal expansion between the fiber and matrix during the composite curing process induce debonding between the fiber and matrix, thereby establishing pathways for oxygen penetration during thermo-oxidative aging[13-14]. Furthermore, oxidation leads to the embrittlement of epoxy resin, promoting the accumulation of microcracks under mechanical loading conditions and exerting a substantial influence on the strength of the epoxy resin[15]. The degradation mechanism is contingent upon the geometry of the specimen and its anisotropic characteristics[16].

There have been several explorations on the effect of thermal aging on compressive behavior[17], tensile behavior[18], torsional behavior[19], impact resistance[20], interlaminar shear strength[21] and short beam shear strength[22]. Gowayed et al.[23] computed the thermal conductivity of four types of plain woven composites using a fabric geometry model. Subsequently, the influence of fiber types and fiber volume fractions on the heat transfer properties was explored. García-Moreno et al.[24-25] investigated the impact and flexural behavior of

Received date: 2024-03-10
Foundation item: National Natural Science Foundation of China (No. 12372130)
* Correspondence should be addressed to GU Bohong, email: gubh@dhu.edu.cn
Citation: SHAKYA P, GU B H. Effect of thermo-oxidative aging on flexural behavior of quasi-isotropic carbon fiber reinforced composite laminates[J]. *Journal of Donghua University (English Edition)*, 2025, 42(3): 259-272.

CFRPs after aging, and a noteworthy increase in flexural strength was observed in specimens aged at a temperature lower than the glass transition temperature T_g. Conversely, a clear deterioration was noted for specimens exposed to higher temperatures. Zhang et al.[9] also reported a significant reduction of the compressive strength in three-dimensional (3D) braided carbon fiber/epoxy specimens caused by aging temperatures near T_g through the finite element model. In contrast, Fiamegkou et al.[26] found a reduction of the interlaminar shear strength in the carbon fiber reinforced cyanate ester laminates. Several investigations have indicated that the degradation of the interface between the fiber and matrix, followed by fiber debonding due to thermal oxidation aging, profoundly affects the failure mechanism of composite materials[27-29].

The aforementioned studies provide evidence that exposure to temperatures above T_g of the material can substantially impact the mechanical properties of CFRPs due to matrix degradation. However, to the best of our knowledge, information on how varying aging durations and composite architectures influence the strength of carbon fiber reinforced epoxy composites is still limited.

This study aims to address the gap by investigating the effects of thermal-oxidative aging over different durations on the flexural behavior of the quasi-isotropic carbon fiber reinforced composite laminate (CFRCL), along with its repercussions on architectural change. Such CFRCL is selected due to its pseudo-ductile behavior[30-31] and relatively uniform mechanical properties. Aging durations ranging from 4 to 32 days are selected and conducted at 180 ℃, which is above the glass transition temperature of the epoxy resin. The flexural strength of both aged and pristine specimens is assessed by the three-point bending test and further analyzed using the finite element method.

1 Materials and Methods

1.1 Materials

The matrix of the CFRCLs is epoxy resin, and the reinforcement is the carbon fibers (SYT49S-12K) with a diameter of 7 μm from Zhongfu Shenying Carbon Fiber Co., Ltd., China. The epoxy resin (JC-02A) and hardener (JC-02B) used for impregnation are from Changshu Jiafa Chemical Inc., China. The physical properties of the reinforcement and matrix are listed in Table 1.

Table 1 Physical properties of reinforcement and matrix

Materials	ρ/(g/cm^3)	E_x/MPa	E_y/MPa ($E_y = E_z$)	ν_{xy} ($\nu_{xy} = \nu_{xz}$)	ν_{yz}	G_{xy}/MPa ($G_{xy} = G_{xz}$)	G_{yz}/MPa
Carbon fiber	1.80	230 000	14 000	0.25	0.3	9 000	5 000
Epoxy resin	1.13	2 400	—	0.35	—	890	—

Notes: ρ is the mass density; E_x, E_y and E_z represent the moduli of elasticity in the longitudinal, transverse and out-of-plane directions, respectively; ν_{xy}, ν_{xz} and ν_{yz} represent the Poisson's ratios in the x-y, x-z and y-z planes, respectively; G_{xy}, G_{xz}, and G_{yz} represent the shear moduli in the x-y, x-z and y-z planes, respectively.

Two sets of quasi-isotropic CFRCLs were fabricated. One was featured by unidirectional carbon fibers, and the other by 1×1 plain woven carbon fibers. The corresponding laminates were named UD-CFRCLs and PW-CFRCLs, respectively. Each of them comprised two distinct configurations. The UD-CFRCLs included UD16 and UD32 specimens which were constructed by stacking 16 and 32 layers of unidirectional carbon fibers, respectively, in a symmetric sequence of 0°, 90°, 45° and −45°. The PW-CFRCLs included PW8 and PW16 specimens which consisted of 8 and 16 layers of plain woven carbon fibers, respectively, arranged in a symmetric sequence of warp, weft, 45° and −45°. The stacking sequences of these laminates are depicted in Fig. 1.

All four laminates (UD16, UD32, PW8 and PW16) were fabricated using the traditional vacuum-assisted resin transfer molding (VARTM) process. They were subjected to a curing process: starting at 90℃ for 2 h, followed by 110℃ for 1 h and concluding with 130 ℃ for 4 h. Subsequently, the laminates were water-jet cut into strips and their edges were polished using sandpaper. The specimens were then prepared according to ASTM D7264 specifications, with a depth-to-span ratio of 1∶20 and a total length equal to 1.2 times the span length. The architecture and dimension parameters of the specimens are summarized in Table 2.

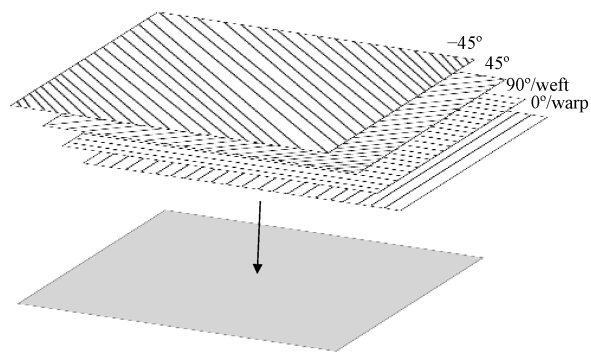

Fig. 1 Stacking sequences of laminates

Table 2 Architecture and dimension parameters of specimens

Specimen		Stacking sequence	Layer	Thickness/mm	Span length/mm	Length×width / (mm×mm)	Fiber volume fraction/%
UD-CFRCLs	UD16	$[0°, 90°, 45°, -45°]_{2s}$	16	3.40	68.0	82.60 × 20	57
	UD32	$[0°, 90°, 45°, -45°]_{4s}$	32	6.80	139.6	167.52 × 20	59
PW-CFRCLs	PW8	$[warp, weft, 45°, -45°]_{1s}$	8	3.74	74.8	89.76 × 20	52
	PW16	$[warp, weft, 45°, -45°]_{2s}$	16	6.87	137.4	164.88 × 20	54

Notes: the subscripts 1, 2 and 4 indicate the sequence is repeated once, twice and four times, respectively; the subscript s means that the entire layup is symmetric (mirrored).

1.2 Thermo-oxidative aging

To simulate long-term thermo-oxidative aging of composites, the specimens underwent thermo-oxidative aging at 180 ℃, a temperature above the glass transition temperature of the resin, for a designated duration of 4, 8, 16 and 32 days. The objective was to ascertain the material's flexural strength under aging conditions. All specimens were then categorized into a total of five groups, comprising the pristine specimen used as a baseline for comparison.

1.3 Quasi-static flexural test

The three-point bending test was performed adhering to ASTM D7264 standard to analyze the flexural properties of the specimens, specifically the maximum strain and maximum flexural stress. The tests were conducted in a universal testing machine (MTS 810, MTS Systems Corporation, USA) equipped with a 100 kN load cell at a stroke rate or crosshead speed of 2.0 mm/min. A schematic depiction of the three-point bending test setup is presented in Fig. 2.

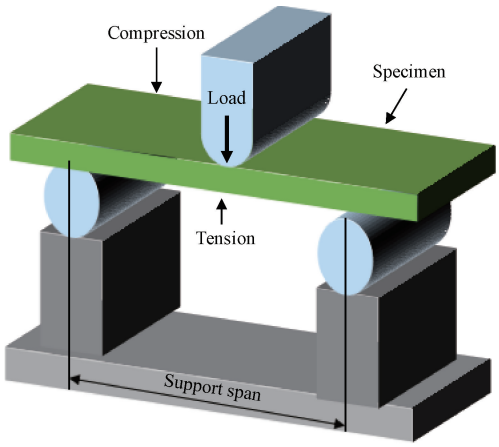

Fig. 2 Schematic diagram of three-point bending test setup

The specimen dimensions in this investigation yield a thickness-to-span length ratio, enabling computation of ultimate flexural stress σ_{max} and flexural strain ε_{max} through the application of Eqs. (1) and (2) adhering to ASTM D7264 standard. This standard is derived from the classical beam theory, predicated on the assumption that shear effects are negligible.

The ultimate flexural stress σ_{max} is expressed as

$$\sigma_{max} = \frac{3F_{max}S}{2bh^2}, \tag{1}$$

where F_{max} is the maximum load at maximum deflection d_{max}; S, b and h are support span, mid-span width and thickness, respectively.

The ultimate flexural strain ε_{max} is expressed as

$$\varepsilon_{max} = \frac{6d_{max}h}{S^2}. \tag{2}$$

1.4 Characterization of aging and flexural damage morphologies

An optical microscope (MI-SIM 2000, CSR Biotech, Guangzhou, China) was employed to characterize the oxidation propagation on the surface of the specimen. Furthermore, failure morphologies after three-point bend loading were compared to elucidate the thermal degradation mechanism of the specimen. Apparent crack propagation occurrences were recorded every second using a digital single-lens reflex (DSLR) camera (HiS-SIM, CSR Biotech, Guangzhou, China) to characterize various failure modes induced by the three-point bending load.

1.5 Numerical simulation

To assess the mechanical behaviors of the composite laminates after thermo-oxidative aging, the specimens with stacking sequences of $[warp, weft, 45°, -45°]_{1s}$ and $[0°, 90°, 45°, -45°]_{2s}$ were modeled in CATIA and ABAQUS software. Figure 3(a) shows an example of the $[0°, 90°, 45°, -45°]_{2s}$ stacking sequence.

The finite element model of the three-point bending test generated in ABAQUS software is shown in Fig. 3(b). The configuration comprises one stroke roller exerting a downward load, the composite laminate and two firm support rollers. The composite laminate consists of resin, fiber reinforcement and fiber/resin interface. Construction of the composite laminate and the rollers utilizes 3D shell elements (SC8R) and 8-node brick elements (C3D8R), respectively. The support rollers were held stationary, whereas the stroke roller had freedom in y direction. Adjustments were made to set up dimensions to align with the actual sizes.

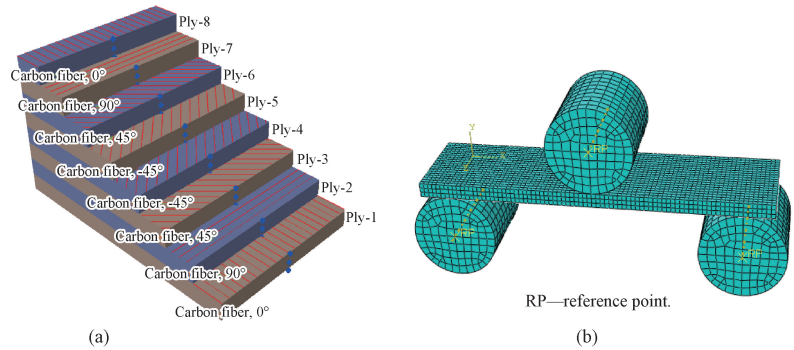

Fig. 3 Finite element models: (a) assembly of laminate with a $[0°, 90°, 45°, -45°]_{1s}$ stacking sequence; (b) three-point bending load simulation

Elastic-plastic behavior of resin is modeled based on the Von Mises yield criterion[32] and expressed as

$$f(\sigma)=\frac{1}{2}\sqrt{(\sigma_1-\sigma_2)^2+(\sigma_2-\sigma_3)^2+(\sigma_3-\sigma_1)^2}-\sigma_s, \quad (3)$$

where σ_1, σ_2, and σ_3 represent the maximal, middle and minimal principal stress components, respectively; σ_s denotes the initial yield stress.

Each composite ply was represented as a homogeneous orthotropic material capable of experiencing progressive damage through the degradation of material stiffness during the resin impregnation and consolidation process. The elastic modulus of all fiber tows was determined by using the bridging model[33]. Attempts were made to correlate the fiber volume fraction with experimental specimens, which had a fiber volume fraction of 52% for the eight-layer PW-CFRCL (PW8) and 57% for the sixteen-layer UD-CFRCL (UD16). Material damage within plies, such as fiber/matrix cracks, was considered to be distributed throughout the volume of the element. The commencement of damage in fiber/matrix was evaluated through the application of ductile and shear failure criteria[34], which were defined by specifying the equivalent plastic strain at the onset of damage and by applying Hashin's criterion. Furthermore, interfacial cohesion between fibers and resin was modeled by using the surface-based cohesive zone model (CZM). Since carbon fibers exhibited relative stability during thermo-oxidative aging and the damage was primarily induced through matrix cracks, the fiber properties were assumed to remain unchanged after thermo-oxidative aging[35]. However, matrix shrinkage induced by thermal oxidation was not considered in this modeling. Only the crack initiations and propagations were considered. Finally, the weakening of the interfaces was characterized by adjusting the parameters in the finite element simulation, utilizing interfacial parameters (Table 3) obtained from Refs. [36-37].

The interaction between yarns and resin was characterized by cohesive behavior. This model is based on bilinear traction law which commences with a linear elastic behavior before damage initiation:

$$\boldsymbol{t}=\boldsymbol{k}_p\boldsymbol{\delta}, \quad (4)$$

where $\boldsymbol{t}$ represents the nominal traction stress vector; $\boldsymbol{k}_p$ is the stiffness matrix; $\boldsymbol{\delta}$ is the strain vector.

Table 3 Interfacial parameters of pristine and aged specimens

Specimen	t_n^0/MPa	$t_s^0 = t_t^0$/MPa	G_n^C/(N·mm)	$G_s^C = G_t^C$/(N·mm)
Pristine	120	150	0.25	1.0
Aged	80	100	0.17	0.67

Notes: t_n^0, t_s^0 and t_t^0 denote the critical stress components at the interface, where t_n^0 represents the normal-direction damage initiation stress, t_s^0 and t_t^0 represent the damage initiation stresses in the primary and secondary tangential direction, respectively; G_n^C, G_s^C and G_t^C denote the work done by the tractions and their conjugate relative displacements in the normal, first and second shear directions, respectively.

Additionally, contact conditions with a friction coefficient of 0.3[21] were incorporated to simulate the interaction between the loading plates and the specimen.

2 Results and Discussion

2.1 Effect of thermo-oxidative aging

Matrix degradation is one of the primary damages caused by aging that can be detected by changes in color in the interlacing areas of the composite. As depicted in Fig. 4, varying color intensities within these interlaced areas correspond to different aging durations, indicative of matrix oxidation. The oxidized areas appear to be darker than the specimen core, and the discoloration extent progressively rises with an increase in aging duration. Before aging, the yarn surface is covered with a thin layer of resin, exhibiting a smooth and glossy texture. However, following aging, oxidation of the resin surface leads to volume shrinkage, while reinforcement positions remain intact. As a result, the resin no longer completely covers the matrix at the yarn interlacing points.

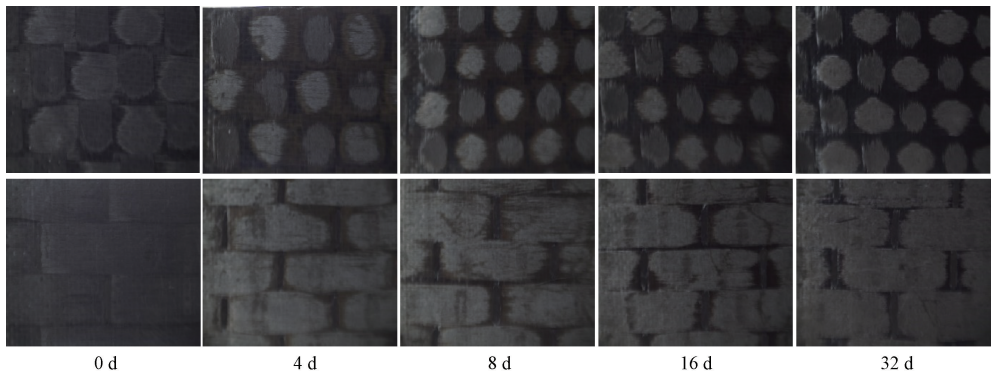

Fig. 4 Oxidation growth in interlacing areas after different aging durations

Figures 5–8 illustrate the interface damage within the fibers and between adjacent layers triggered by thermo-oxidative aging. The cracks upon aging are visible in 16-day-aged PW8, UD16 and PW16, as well as in 8-day-aged UD32. The emergence of fissures gives rise to extra surfaces and pathways that facilitate the transport of oxygen into the inner layers of the composite material.

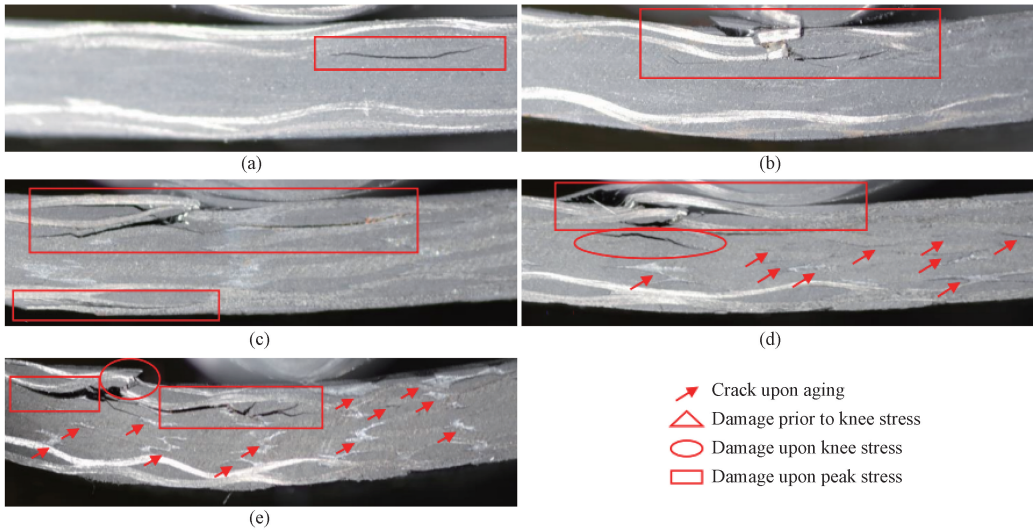

Fig. 5 Damage in PW8 laminates after different aging durations: (a) 0 d; (b) 4 d; (c) 8 d; (d) 16 d; (e) 32 d

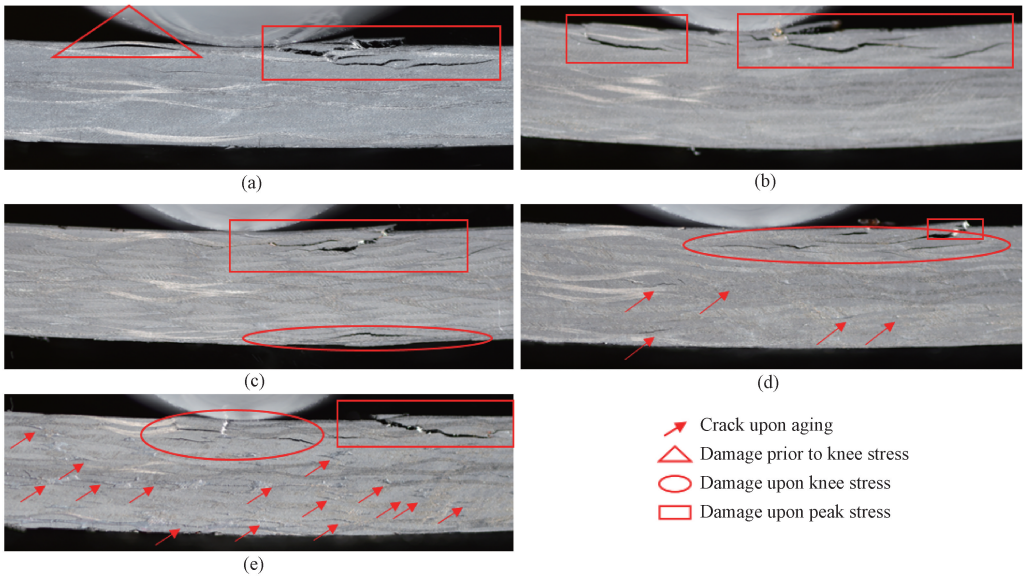

Fig. 6 Damage in PW16 laminates after different aging durations: (a) 0 d; (b) 4 d; (c) 8 d; (d) 16 d; (e) 32 d

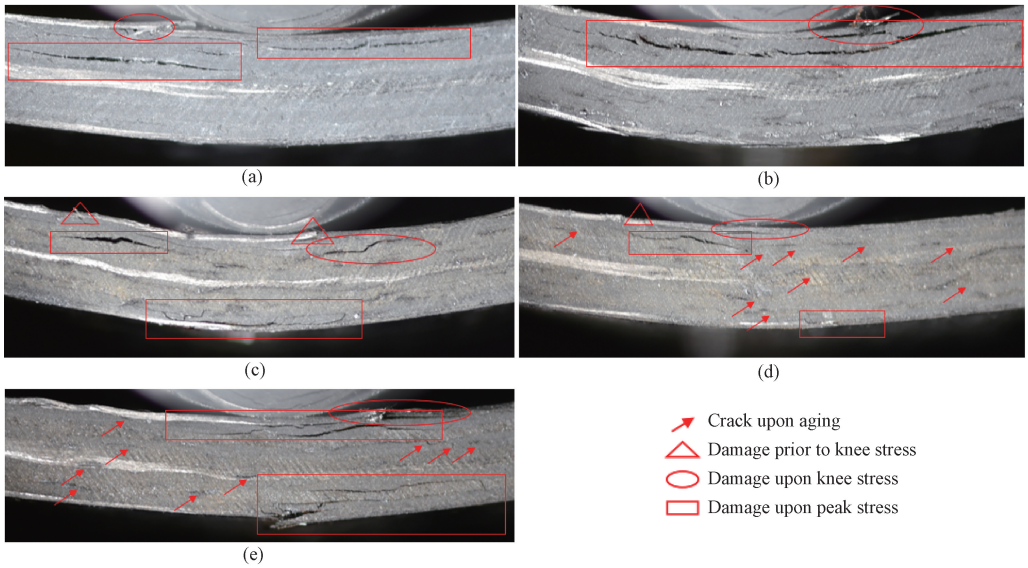

Fig. 7 Damage in UD16 laminates after different aging durations: (a) 0 d; (b) 4 d; (c) 8 d; (d) 16 d; (e) 32 d

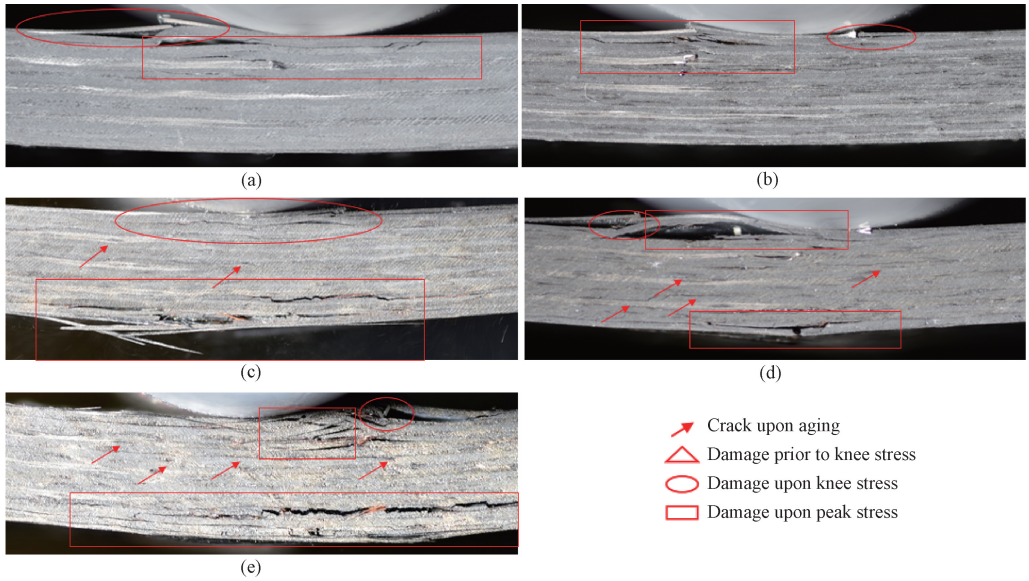

Fig. 8 Damage in UD32 laminates after different aging durations: (a) 0 d; (b) 4 d; (c) 8 d; (d) 16 d; (e) 32 d

The crack propagation preferentially occurs in the direction of the fibers, especially along the interface between the fiber and the matrix, leading to the formation of the most profound zone of fractures. Ongoing extension of crack propagation was anticipated as the aging time was prolonged.

2.2 Flexural behavior and damage analysis

2.2.1 Knee point stress

A knee point emerges at the elastic limit, serving as a transition between the linear and non-linear stress-strain relationship, marking the initiation of damage in the experimental specimen[38]. The flexural knee point stress for all four specimens (summarized in Table 4) indicates that knee point stress did not manifest in thinner samples until 16 days of aging, while it was evident in pristine thicker specimens. The results suggest a consistent degradation in knee point stress as laminate thickness and aging duration increase.

Table 4 Knee point stress and ultimate stress of four specimens at different aging durations

Aging duration/d	Knee point stress/MPa				Ultimate stress/MPa			
	PW8	UD16	PW16	UD32	PW8	UD16	PW16	UD32
0	—	—	604.77	524.56	783.59	488.86	648.89	532.02
4	—	—	560.42	469.35	772.82	483.29	625.17	515.00
8	—	—	459.40	412.75	747.82	470.55	578.77	455.99
16	617.71	411.61	429.02	412.77	664.09	458.19	572.80	426.53
32	534.26	297.44	421.22	393.90	595.52	445.29	549.83	393.90

2.2.2 Flexural strength

The flexural strength characterizes the ability of laminated composites to endure bending stresses before the fracture point. Common failure modes under flexural loading encompass compressive, tensile and/or shear failure, which are linked with phenomena such as matrix cracking, fiber breakage and delamination. The tests on pristine specimens were performed to determine the flexural behavior of all specimens. The flexural strength was determined by the ultimate stress before failure. The flexural strength values of the specimens (PW8, PW16, UD16 and UD32 with fiber volume fractions of 52%, 54%, 57% and 59%, respectively) are presented in Fig. 9. Both the flexural strength of PW-CFRCLs and UD-CFRCLs decreased after aging. After 8 days of aging, the flexural strength of PW8 and PW16 decreased by 5% and 4%, respectively, while that of UD16 and UD32 decreased by 11% and 14%, respectively. The flexural strength of PW8 is higher than that of UD16, regardless of the lower fiber content in UD16. This indicates the superior performance of PW-CFRCLs compared to UD-CFRCLs. For pristine specimens, the flexural strength reaches 783.59 MPa for PW8 and 648.89 MPa for UD16, which gradually decreases with an increase in aging duration. The minimum flexural strength of PW8 and UD16 is observed upon 32 days of aging, measuring 595.52 MPa and 549.83 MPa, respectively. As anticipated, the ultimate flexural stress of the specimens depicted a gradual reduction with an increase in aging duration. Furthermore, all pristine specimens failed on the compressive layer, while the tensile failure could be seen in the aged thicker laminates.

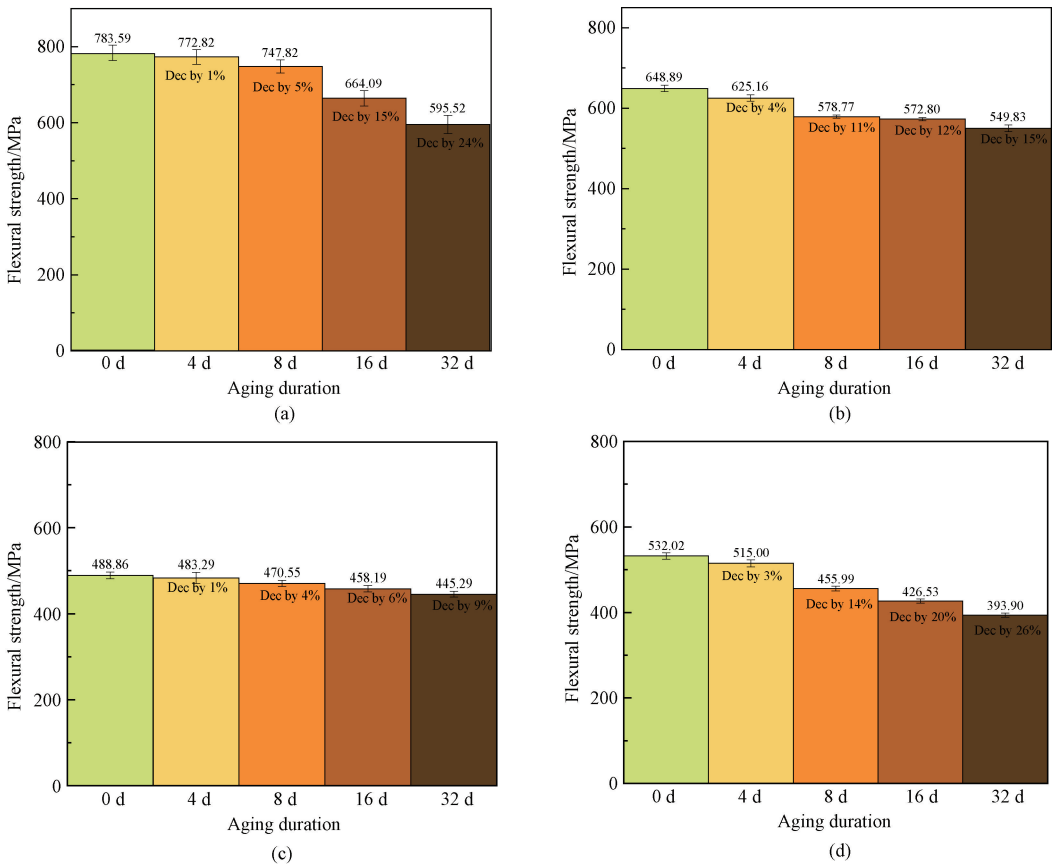

Dec—decreased.

Fig. 9 Flexural strength of specimens as a function of aging duration: (a) PW8; (b) UD16; (c) PW16; (d) UD32

2.2.3 Effect of thermo-oxidative aging on PW-CFRCLs

To examine the influence of thermo-oxidative aging on the flexural damage response concerning material thickness, two PW-CFRCLs with the same architecture, but a distinct number of plies were investigated. The effect of aging on flexural resistance was assessed by using maximum flexural strength as a metric. Additionally, microscopic views of the damage were captured through the DSLR camera during the test. The flexural strength as a function of the thermo-oxidative aging duration for PW8 and PW16 is shown in Fig. 9, while the stress-deflection curves for both samples are presented in Fig. 10.

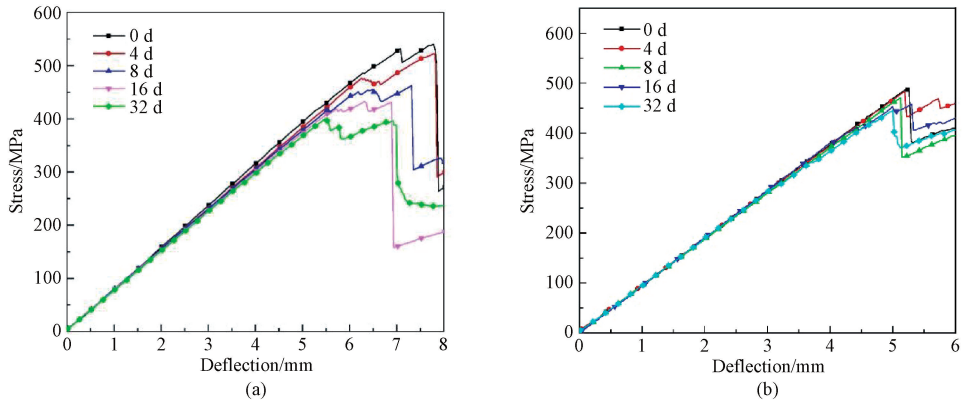

Fig. 10 Flexural stress-deflection curves of specimens after different aging durations: (a) PW8; (b) PW16

The results indicate that the ultimate flexural stress of specimens upon aging reduced gradually with an increase in aging duration. This is mainly attributed to molecular configuration accompanied by thermal deterioration, leading to embrittlement of the epoxy resin[39-40]. Furthermore, the flexural strengths of PW8 (a thickness of 3.7 mm) and PW16 (a thickness of 6.8 mm) are 783.59 MPa and 488.86 MPa, respectively. This represents a 38% reduction in flexural strength for the thicker laminate (PW16) compared to the thinner counterpart (PW8).

This result demonstrates that thinner specimens exhibit superior flexural performance, potentially attributed to dry fiber bundles within thicker laminates creating weakly bonded interfaces, thereby reducing load transfer efficiency. If a lack of guaranteed interfacial adhesion at an interface exists, then the efficient transfer of stress throughout the interface will be inhibited. As a result, the mechanical performance of the resulting composite can be significantly restricted due to the extremely low-stress transfer efficiency[41]. Additionally, the thicker laminate was not as prone to thermal-oxidative aging as the thinner laminate in terms of flexural strength, as the ultimate stress of PW8 decreased by 24% after 32 days of aging, while that of PW16 decreased by merely 9%.

Crack initiation in both PW8 and PW16 occurred in the compressive side layer (Figs. 5 and 6), which is close to the applied load at an initial stage, gradually progressing inwards upon an increase in aging duration. However, the interface crack on the tension side could also be seen on the 8-day-aged PW16. At the early stage of aging (0–8 d), the failure was dominated by matrix cracking and fiber kinking. With the increase of aging time (16–32 d), in addition to cracks formed by the thermo-oxidative process, matrix cracks upon load occurred just after the knee point, which led to further stiffness degradation in the flexural stress-deflection relation diagram (Fig. 10). Fiber/matrix debonding and intralaminar cracks on the other hand can be observed before the peak point. The reduction in flexural strength might be attributed to crack propagation caused by oxidative aging-induced matrix and fiber/matrix interface degradation. Moreover, only the outer layer of the specimens was fractured, while the inner core remained intact despite exhibiting minor cracks upon aging. This could be due to the limited thickness of the oxidized layer within the surface region, which protected the inner epoxy from further oxidation[42].

In pristine PW8 specimens, the presence of a matrix crack in the second layer became apparent upon reaching peak stress. Subsequently, after 4 to 8 days of aging, these cracks elongated, accompanied by the emergence of an additional crack on the first layer. Additionally, the phenomenon of fiber/matrix debonding and fiber kinking can be observed. The manifestation of cracks attributed to aging became apparent after 16 days of aging, resulting in further fiber/matrix debonding on the third layer. After the final stage (32 d), the visibility of aging-induced cracks heightened, with an intensified severity of fiber/matrix cracks. Furthermore, yarn breakage was discernible on the first two layers. PW16 exhibited a similar pattern to PW8, nevertheless, cracks were noticeable upon reaching knee stress, and the intensity and quantity of fiber/matrix debonding were augmented.

2.2.4 Comparison of thermo-oxidative aging effects on PW-CFRCLs and UD-CFRCLs

In an attempt to compare the effect of fabric structure on the material subjected to thermal-oxidative aging, PW-CFRCLs were compared with UD-CFRCLs of

similar thicknesses. In terms of architecture, PW8 exhibited slightly higher flexural strength (783.59 MPa) than UD16 (648.89 MPa). Even after aging for 32 days, the flexural strength of PW8 (595.52 MPa) was still superior to that of UD16 (549.83 MPa). In the thicker laminates, although the pristine UD32 initially exhibited higher flexural strength than PW16, it was more susceptible to thermal-oxidative aging. Ultimately, the flexural strength of PW16 decreased by 9% after 32 days of aging, while that of UD32 decreased by 26% (Fig. 9). This result indicates that PW-CFRCLs are more suitable for application in heat than UD-CFRCLs.

Both compressive and tensile failures of UD-CFRCLs were observed after aging. Similar to PW-CFRCLs, the thinner UD-CFRCL performed better than the thicker one. UD16 exhibited a linear stress-deflection relationship up to the maximum stress, however, an obvious dip in flexural stress could be seen in UD32 before failure (Fig. 11). Unidirectional laminates showed brittle behavior, with matrix cracking initiating on the first two layers on the compressive side. These matrix cracks initiated at the knee stress point and then moved catastrophically through the specimen, leading to delamination and fiber breakage in the aged specimen. Matrix cracks could also be seen after 16 days of aging. In addition to the cracks formed by the thermo-oxidative process, load-induced matrix cracks occurred, which further degraded the stiffness in the flexural stress-deflection relationship. Matrix cracking and delamination occurred in the 90° layer, while the fiber breakage was observed in the 0° layer.

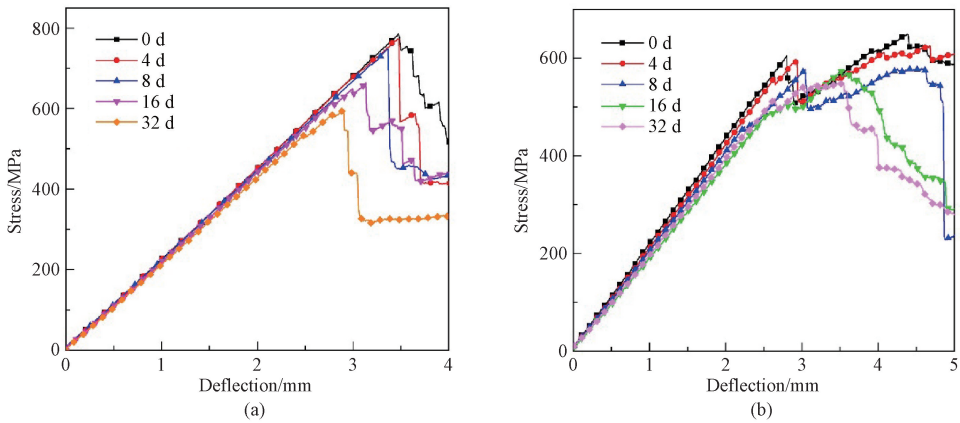

Fig. 11 Flexural stress-deflection curves of specimens after different aging durations: (a) UD16; (b) UD32

2.3 Finite element analysis

A numerical model for the aged laminate was established according to the morphology and property characterization of the laminates after thermo-oxidative aging. The model incorporates consideration of thermo-oxidative degradation of both the matrix and the interface. The main purpose of the simulation was to provide insight into the qualitative results of three-point bending tests conducted on quasi-isotropic materials. Moreover, aging for 16 and 32 days was selected because no apparent degradation was observed after 4 and 8 days of aging.

Figures 12 and 13 depict the stress-deflection curves of PW8 and UD16, comparing those obtained from the numerical results and the experimental results. The numerical results show a good correlation with the experimental results.

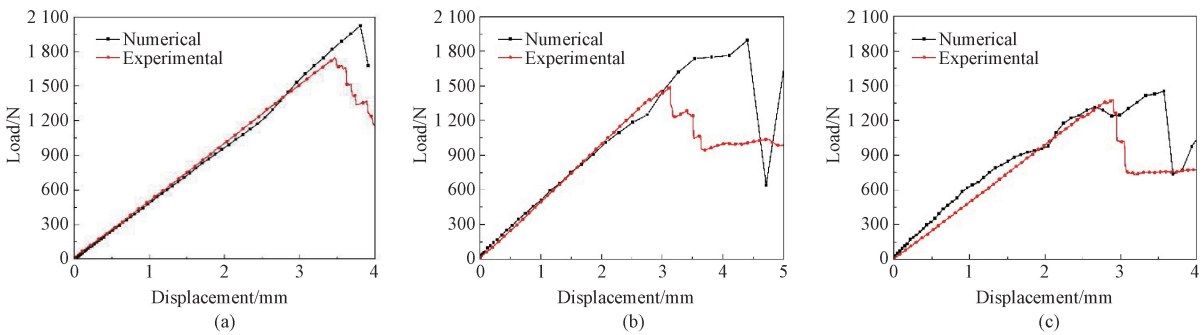

Fig. 12 Comparison of ultimate load between numerical and experimental data of PW8 after different aging durations: (a) 0 d; (b) 16 d; (c) 32 d

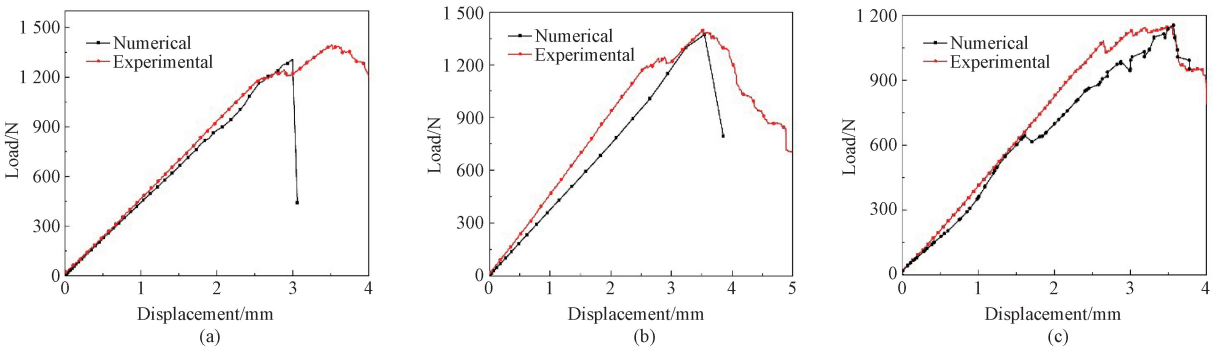

Fig. 13 Comparison of ultimate load between numerical and experimental data of UD16 after different aging durations: (a) 0 d; (b) 16 d; (c) 32 d

Figures 14 and 15 illustrate the damage progression of the laminates subjected to aging. Interface cracks initiate at the surface and propagate towards the core, while only matrix degradation is considered in the inner core. In PW8 laminate, only matrix cracks are apparent in pristine specimens. The damage is initiated under the crosshead after fiber kinks in the bottom layer, ultimately leading to failure in the entire specimen. UD 16 laminate undergoes fiber/matrix debonding even in the pristine specimens, and this phenomenon propagates with increasing aging duration.

The flexural behavior of both pristine and aged specimens was corroborated through a specimen-scale model. The finite element model aptly anticipates the distinct failure modes observed in experimental observations. Furthermore, the stress distribution and interface damage were discerned at the peak load and knee point, respectively, elucidating the underlying mechanisms of damage. In pristine PW8 specimens, only matrix cracks were evident, while interface damage commenced in the 16-day and 32-day aged specimens after fiber breakage in the bottom layer. Figures 14 and 15 display the plots from the finite element analysis (FEA) of aged laminates, illustrating the failed elements in the FEA mesh. Notably, the pristine specimens failed due to matrix cracking, while the aged specimens experienced failure due to interface damage. Conversely, in UD16 laminates, interface damage is observable in the pristine specimens and the aged specimens.

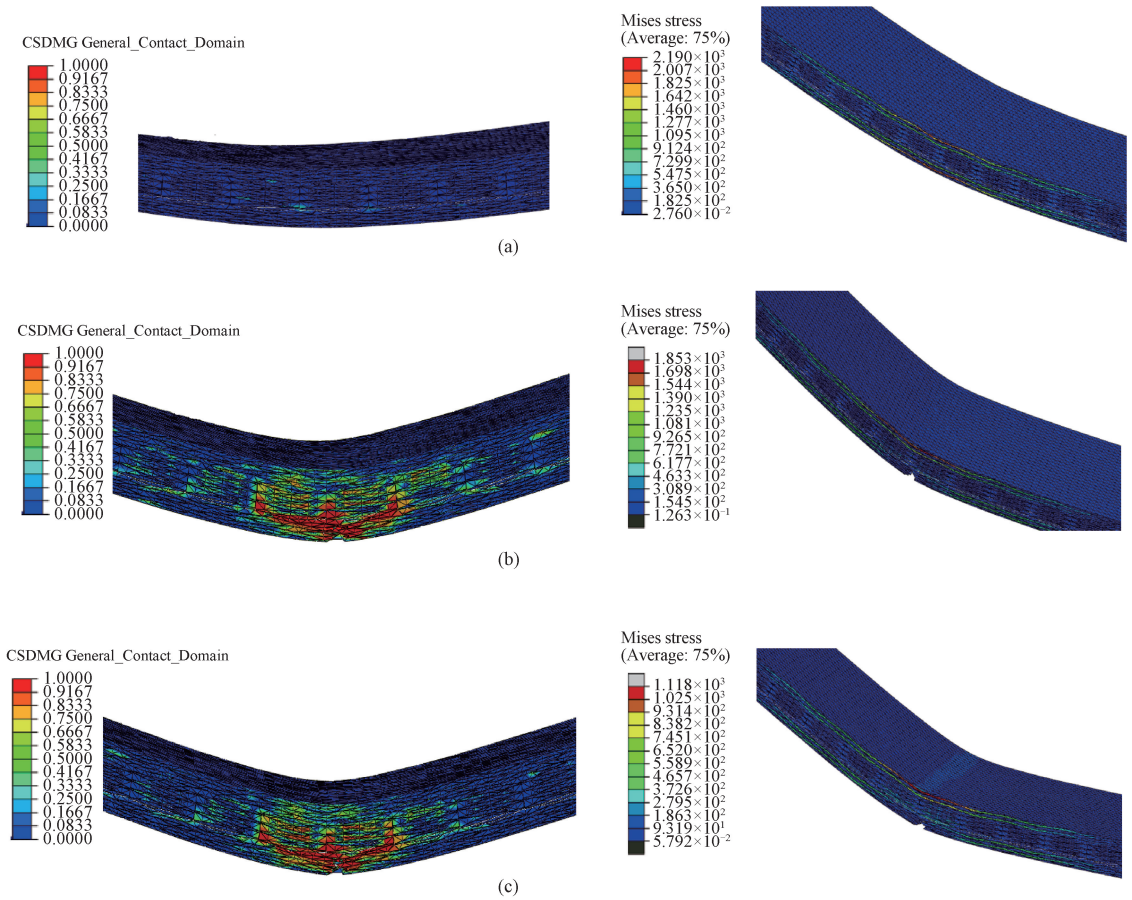

Fig. 14 Numerical damage and stress level of PW8 after different aging durations: (a) 0 d; (b) 16 d; (c) 32 d

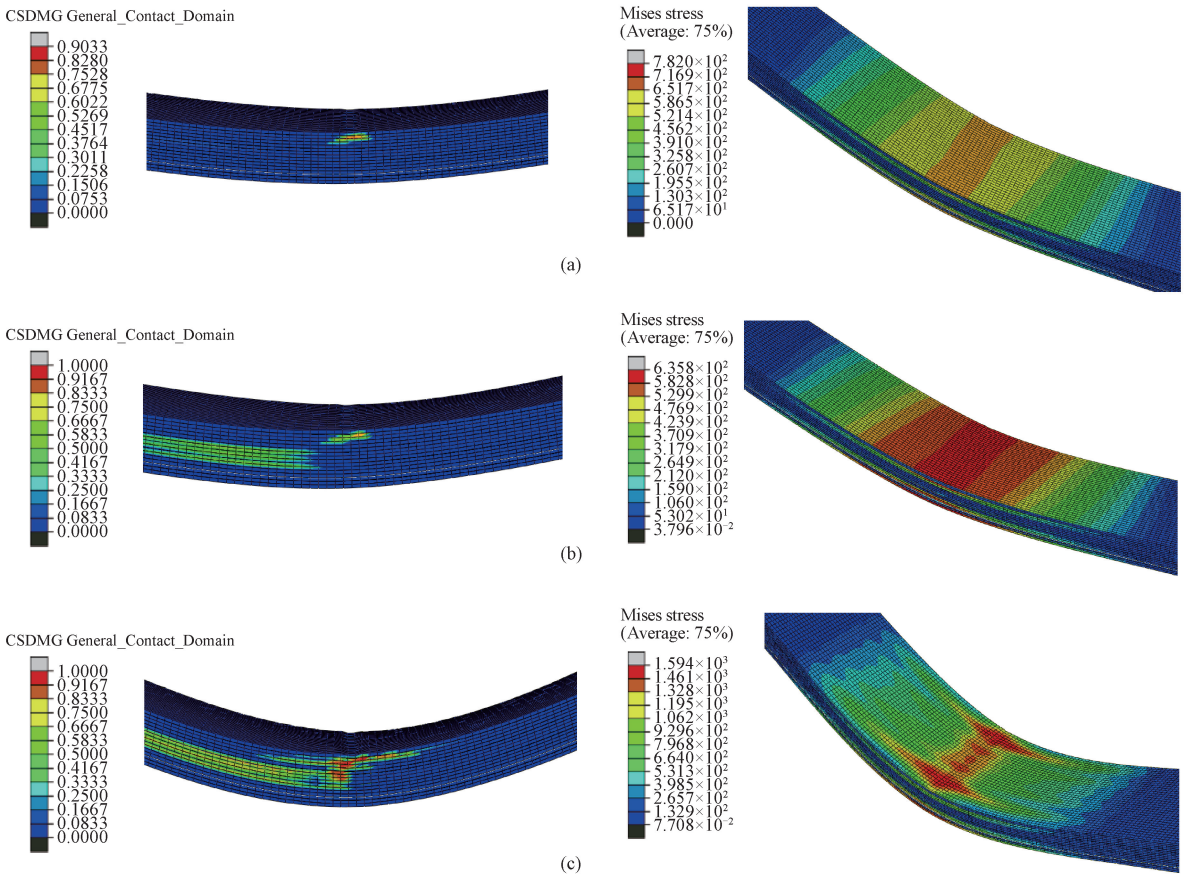

Fig. 15 Numerical damage and stress level of UD16 after different aging durations: (a) 0 d; (b) 16 d; (c) 32 d

3 Conclusions

This study investigated the impact of thermo-oxidative aging at various durations on the flexural behavior of quasi-isotropic PW-CFRCLs, contrasting their performance with that of quasi-isotropic UD-CFRCLs. In addition, the finite element method was employed to validate the experimental results in assessing the flexural behavior of the laminates. We found that flexural strength decreased with the increase in aging duration. Furthermore, fabric architecture significantly influenced flexural performance, and increasing laminate plies did not substantially enhance flexural strength. Matrix cracking and fiber/matrix debonding were the primary causes of failure in all four specimens, however, fiber breakage was observed in PW-CFRCLs upon aging and an additional delamination in unidirectional laminates. These phenomena are supported by numerical analysis, which indicates the superiority of plain woven composite over unidirectional laminates and the degradation of flexural strength with an increase in aging duration. We hope such a model could be extended to design at the meso- and microscale as well as for other composite structures with excellent thermo-oxidative aging resistance, particularly for aerospace applications. Overall, the findings serve as the foundation for further analyses to enable integrity assessments and damage mode identification by using the finite element method for asymmetric plain woven and unidirectional composites.

References

[1] LI Z, HAIGH A, SOUTIS C, et al. Detection and evaluation of damage in aircraft composites using electromagnetically coupled inductors[J]. *Composite Structures*, 2016, 140: 252-261.

[2] SARFRAZ M S, HONG H, KIM S S. Recent developments in the manufacturing technologies of composite components and their cost-effectiveness in the automotive industry: a review study[J]. *Composite Structures*, 2021, 266: 113864.

[3] SHI Y, SOUTIS C. Modelling transverse matrix cracking and splitting of cross-ply composite laminates under four point bending[J]. *Theoretical and Applied Fracture Mechanics*, 2016, 83: 73-81.

[4] SOUTIS C. Fibre reinforced composites in aircraft construction[J]. *Progress in Aerospace*

Sciences, 2005, 41(2): 143-151.
[5] JIN X C, FAN X L, LU C S, et al. Advances in oxidation and ablation resistance of high and ultra-high temperature ceramics modified or coated carbon/carbon composites[J]. *Journal of the European Ceramic Society*, 2018, 38(1): 1-28.
[6] WU D F, LIN L J, REN H Y, et al. High-temperature deformation measurement of the heated front surface of hypersonic aircraft component at 1 200 ℃ using digital image correlation[J]. *Optics and Lasers in Engineering*, 2019, 122: 184-194.
[7] WANG L, SUN B Z, GU B H. Mode-I fracture crack growth behaviors of 3-D angle interlock woven composites under low-velocity wedge-loaded impact [J]. *Engineering Fracture Mechanics*, 2021, 242: 107468.
[8] TATLıDILLI A, ÇETIN ALTıNDAL D, GÜMÜŞDERELIOĞLU M. Effects of carbon fiber type and resin ratio on thermal and mechanical lifetime of polyetherimide composites [J]. *Polymer Composites*, 2021, 42(6): 2920-2932.
[9] ZHANG M, SUN B Z, GU B H. Experimental and numerical analyses of matrix shrinkage and compressive behavior of 3-D braided composite under thermo-oxidative ageing conditions [J]. *Composite Structures*, 2018, 204: 320-332.
[10] SHI B H, ZHANG M, LIU S K, et al. Multi-scale ageing mechanisms of 3D four directional and five directional braided composites' impact fracture behaviors under thermo-oxidative environment [J]. *International Journal of Mechanical Sciences*, 2019, 155: 50-65.
[11] TSOTSIS T K, LEE S M. Long-term thermo-oxidative aging in composite materials: failure mechanisms [J]. *Composites Science and Technology*, 1998, 58(3/4): 355-368.
[12] UPADHYAYA P, SINGH S, ROY S. A mechanism-based multi-scale model for predicting thermo-oxidative degradation in high temperature polymer matrix composites [J]. *Composites Science and Technology*, 2011, 71(10): 1309-1315.
[13] HAQUE M H, UPADHYAYA P, ROY S, et al. The changes in flexural properties and microstructures of carbon fiber bismaleimide composite after exposure to a high temperature [J]. *Composite Structures*, 2014, 108: 57-64.
[14] VARGHESE J, WHITCOMB J. Micromechanics of oxidation in composites with impermeable fibers [J]. *Journal of Composite Materials*, 2009, 43(19): 2011-2043.
[15] ODEGARD G M, BANDYOPADHYAY A. Physical aging of epoxy polymers and their composites[J]. *Journal of Polymer Science Part B: Polymer Physics*, 2011, 49(24): 1695-1716.
[16] GIGLIOTTI M, PANNIER Y, MINERVINO M, et al. The effect of a thermo-oxidative environment on the behaviour of multistable [0/90] unsymmetric composite plates [J]. *Composite Structures*, 2013, 106: 863-872.
[17] FAN W, GUO D D, LI J L, et al. Effect of thermo-oxidative aging on compressive behavior of carbon fiber polymer matrix composites [J]. *Textile Research Journal*, 2018, 88(5): 510-519.
[18] SUN G Y, ZUO W, CHEN D D, et al. On the effects of temperature on tensile behavior of carbon fiber reinforced epoxy laminates [J]. *Thin-Walled Structures*, 2021, 164: 107769.
[19] XUN L M, WU Y Y, HUANG S W, et al. Degradation of torsional behaviors of 3-D braided thin-walled tubes after atmospheric thermal ageing [J]. *Thin-Walled Structures*, 2022, 170: 108555.
[20] YANG Y, XU F, GAO X Y, et al. Impact resistance of 2D plain-woven C/SiC composites at high temperature [J]. *Materials & Design*, 2016, 90: 635-641.
[21] GUO F L, HUANG P, LI Y Q, et al. Multiscale modeling of mechanical behaviors of carbon fiber reinforced epoxy composites subjected to hygrothermal aging [J]. *Composite Structures*, 2021, 256: 113098.
[22] CAO M, GAO X Z, TANG B L, et al. Multiscale thermal oxidative ageing mechanisms of carbon fiber/epoxy plain woven composites under short beam shear loading[J]. *Thin-Walled Structures*, 2023, 185: 110566.
[23] GOWAYED Y, HWANG J C. Thermal conductivity of composite materials made from plain weaves and 3-D weaves [J]. *Composites Engineering*, 1995, 5(9): 1177-1186.
[24] GARCÍA-MORENO I, CAMINERO M Á, RODRÍGUEZ G P, et al. Effect of thermal ageing on the impact and flexural damage behaviour of carbon fibre-reinforced epoxy laminates[J]. *Polymers*, 2019, 11(1): 80.
[25] GARCÍA-MORENO I, CAMINERO M Á, RODRÍGUEZ G P, et al. Effect of thermal ageing on the impact damage resistance and tolerance of carbon-fibre-reinforced epoxy laminates[J]. *Polymers*, 2019, 11(1): 160.
[26] FIAMEGKOU E, KOLLIA E, VAVOULIOTIS A, et al. The effect of thermo-oxidative aging on carbon fiber reinforced cyanate ester composites [J]. *Journal of Composite Materials*, 2015, 49

(26): 3241-3250.

[27] DA SILVA L V, DA SILVA F W, TARPANI J R, et al. Ageing effect on the tensile behavior of pultruded CFRP rods[J]. *Materials & Design*, 2016, 110: 245-254.

[28] CAO M, WANG H L, GU B H, et al. Impact damage and compression behaviours of three-dimensional angle-interlock woven composites after thermo-oxidation degradation[J]. *Journal of Composite Materials*, 2018, 52(15): 2085-2101.

[29] MOUZAKIS D E, DIMOGIANOPOULOS D G, ZAOUTSOS S. Damage assessment of carbon fiber reinforced composites under accelerated aging and validation *via* stochastic model-based analysis[J]. *International Journal of Damage Mechanics*, 2014, 23(5): 702-726.

[30] MUJIKA F. On the effect of shear and local deformation in three-point bending tests[J]. *Polymer Testing*, 2007, 26(7): 869-877.

[31] VARNA J, JOFFE R, AKSHANTALA N V, et al. Damage in composite laminates with off-axis plies[J]. *Composites Science and Technology*, 1999, 59(14): 2139-2147.

[32] CHEN J L, SUN C T. A plastic potential function suitable for anisotropic fiber composites[J]. *Journal of Composite Materials*, 1993, 27(14): 1379-1390.

[33] HUANG Z M. A unified micromechanical model for the mechanical properties of two constituent composite materials. Part I: elastic behavior[J]. *Journal of Thermoplastic Composite Materials*, 2000, 13(4): 252-271.

[34] HOOPUTRA H, GESE H, DELL H, et al. A comprehensive failure model for crashworthiness simulation of aluminium extrusions[J]. *International Journal of Crashworthiness*, 2004, 9(5): 449-464.

[35] ZHANG M, SUN B Z, GU B H. Meso-structure ageing mechanism of 3-D braided composite's compressive behaviors under accelerated thermo-oxidative ageing environment[J]. *Mechanics of Materials*, 2017, 115: 47-63.

[36] CAO M, GU B H, SUN B Z. Low-velocity impact and residual flexural behaviors of 2.5-D woven composite under accelerated thermal ageing: experiment and numerical modelling[J]. *International Journal of Damage Mechanics*, 2020, 29(3): 413-434.

[37] KE Y N, HUANG S W, GUO J H, et al. Effects of thermo-oxidative aging on 3-D deformation field and mechanical behaviors of 3-D angle-interlock woven composites[J]. *Composite Structures*, 2022, 281: 115116.

[38] PANDITA S D, HUYSMANS G, WEVERS M, et al. Tensile fatigue behaviour of glass plain-weave fabric composites in on- and off-axis directions[J]. *Composites Part A: Applied Science and Manufacturing*, 2001, 32(10): 1533-1539.

[39] BARBOSA A P C, FULCO A P P, GUERRA E S S, et al. Accelerated aging effects on carbon fiber/epoxy composites[J]. *Composites Part B: Engineering*, 2017, 110: 298-306.

[40] ERNAULT E, RICHAUD E, FAYOLLE B. Origin of epoxies embrittlement during oxidative ageing[J]. *Polymer Testing*, 2017, 63: 448-454.

[41] MA Y, UEDA M, YOKOZEKI T, et al. A comparative study of the mechanical properties and failure behavior of carbon fiber/epoxy and carbon fiber/polyamide 6 unidirectional composites[J]. *Composite Structures*, 2017, 160: 89-99.

[42] ZHANG M, SUN B Z, GU B H. Accelerated thermal ageing of epoxy resin and 3-D carbon fiber/epoxy braided composites[J]. *Composites Part A: Applied Science and Manufacturing*, 2016, 85: 163-171.

准各向同性碳纤维层合板弯曲性的热氧化效应

SHAKYA Priyanka, 顾伯洪*
东华大学 纺织学院, 上海市现代纺织前沿科学研究基地, 上海 201620

摘　要: 随着碳纤维增强聚合物（carbon fiber reinforced polymers, CFRPs）在高温度环境中应用日益广泛, 研究其对材料性能的影响变得至关重要。该研究对准各向同性平纹和单向碳纤维增强层压板的弯曲强度进行了热氧化老化影响的研究与对比, 即对试样进行了不同时间的热氧化老化处理, 并通过三点弯曲试验对其弯曲强度进行了评估。结果证明层压板的弯曲强度随老化时间的延长而降低。值得注意的是, 尽管平纹复合层压板的纤维含量较低, 但其弯曲强度却高于单向复合层压板。经过 8 d 的老化, 平纹板的弯曲强度仅下降了 4%~5%, 而单向板则下降了 11%~14%。经过 32 d 的老化后, 弯曲强度最高（595.52 MPa）的是最低纤维含量的较薄平纹复合层压板, 其次是薄单向复合层压板（549.83 MPa), 然后是厚平纹复合层压板（445.29 MPa), 最低的是厚单向复合层压板（393.90 MPa)。层压板弯曲性能的下降主要归因于基体氧化引起的基体裂纹和界面脱粘。为了验证结果的普遍性, 该研究采用了有限元方法进行模拟, 结果与试验数据相符。

关键词: 抗弯强度; 热氧化老化; 基体氧化; 界面脱粘; 有限元方法